International Journal of Sustainable and Green Energy
2021; 10(4): 129-144
http://www.sciencepublishinggroup.com/j/ijsge
doi: 10.11648/j.ijrse.20211004.13
ISSN: 2575-2189 (Print); ISSN: 2575-1549 (Online)

Performance Analysis of Foam Ice Production System with Direct Contact Refrigerant Spraying in PCM Material Based on Dynamic Two-stage Refrigeration Cycle Driven by DPES

Yongfeng Xu[1, 2], Guoliang Li[1, 3], Ming Li[1, 3, *]

[1]Solar of Energy and Environment Science, Yunnan Normal University, Kunming, China

[2]College of Information Science and Engineering, Jiaxing University, Jiaxing, China

[3]Key Laboratory of Solar Heating and Cooling Technology of Yunnan Provincial Universities, Kunming, China

Email address:

lmllldy@126.com (Ming Li)

[*]Corresponding author

To cite this article:

Yongfeng Xu, Guoliang Li, Ming Li. Performance Analysis of Foam Ice Production System with Direct Contact Refrigerant Spraying in PCM Material Based on Dynamic Two-stage Refrigeration Cycle Driven by DPES. *International Journal of Sustainable and Green Energy*. Vol. 10, No. 4, 2021, pp. 129-144. doi: 10.11648/j.ijrse.20211004.13

Received: October 31, 2021; **Accepted**: November 22, 2021; **Published**: December 2, 2021

Abstract: A 2kW dynamic two-stage refrigerant direct injection refrigeration system directly driven by distributed PV energy was investigated by combining experiment and simulation. The simulation results were in good agreement with the experimental data with -1.03% relative error of instantaneous generation power and 5.16% relative error of COP. And then, the refrigeration performance of R22, R134a and R318 were tested and the average COPs were 6.16, 5.80 and 8.70, respectively. More importantly, relatively environmentally friendly refrigerants R407C and R410a had better refrigeration performance and the COPs were 6.13 and 8.52. Finally, the dynamic performance parameters of refrigerant injection and the influence of component parameters on refrigeration COP were analyzed. The wall thickness of the plate heat exchanger had a negative effect on the heat transfer coefficient of the exchanger and the COP of the second refrigeration system. The average increase rates were - 0.234 kW/(m^2°C) and -0.017. The exchange area of exchanger had a positive effect on the COP and refrigerant mass flow of the second refrigeration system. The average increase rates were 12.92 m^{-2} and 0.0209 kg/(s·m^2). Moreover, the effect of refrigerant injection speed on refrigeration performance, COP and outlet refrigerant temperature, was greater than that of injection pressure. Changing capillary inner diameter had a greater effect on the refrigeration performance than changing the length of capillary. Therefore, it was faster to optimize the refrigerant the refrigerant direct injection refrigerant performance by adjusting the capillary inner diameter.

Keywords: Refrigerant Direct Injection Refrigeration System, Foam Ice, Distributed Photovoltaic Energy System, Capillary

1. Introduction

The relation between power supply and refrigeration demand is becoming more and more intense for the rapid development of economy and living standard. So cold storage air-conditioning unit had been widely adopted for the electric power peak-load shifting [1]. Phase change materials (PCM) such as water, inorganic salts, organic alcohols and gas hydrates, with stable performance and high latent heat value were employed in heat energy storage [2-5]. But the refrigeration efficiency and super-cooling of PCMs were the focus and hotspot of researchers [6-10]. So the direct contact heat exchanger and ice slurry were the practical solutions for the super-cooling of PCMs cold storage. The direct contact heat exchangers had many undoubted advantages for the absence of the internals or barriers between refrigerant and PCMs thermal storage over surface type heat exchangers such as shell and tube [11]. Because in ice-on-coil system, the evaporator coil was submerged in the PCMs thermal storage and the ice was formed around the coil. For the poor thermal conductively of ice, the refrigeration efficiency gradually reduced along with the increase of the ice thickness [12, 13].

Therefore, in order to improve the refrigeration efficiency, the refrigeration technology of direct contact heat transfer is proposed, which is that the refrigerant is sprayed into cold storage material and the heat transfer is efficient without intermediate thermal resistance [14-17]. When R12 was employed as the refrigerant, the heat transfers between R12 and water was close to 100% and the system COP was about 3.4-3.6 [18, 19], which was almost about 2-3 times that of coil evaporator ice making system. Because direct contact heat transfer keeps in contact with immiscible continuous liquid without intermediate thermal resistance, which is widely used in many industrial fields, such as industrial energy recovery and thermal energy storage for the advantages of relatively simple design, high heat transfer coefficient and no installation.

Moreover, in cold storage system, slurry ice was attractive for excellent thermal storage property and lower super-cooling degree [20]. Ice slurry has good fluidity, when it was employed as refrigerant in transporting cooling capacity process, its cooling density was several times that of traditional refrigerant carrier. So the flow of ice slurry was smaller and the power consumed was lower. Moreover, the ice slurry has a lower flower resistance and larger heat transfer coefficient than cold water [19]. There are six methods to generate ice slurry such as moving bed, super-cooling, scraped surface heat exchanger, evaporative super-cooling, vacuum ice making and direct contact heat transfer. Among them, direct contact refrigeration with refrigerant injection has the advantages of low super-cooling and high refrigeration efficiency, which has attracted the attention of researchers.

The formation mechanism, the influence of ice crystal size on the fluidity and heat transfer performance and the ice point drift characteristics of ice slurry in refrigerant injecting process were investigated in detail [21]. The research on the performance of direct contact evaporation heat transfer mainly focused on single droplet evaporation. Refrigerant droplet gradually absorbed heat and vaporized in PCM energy storage material, the droplet volume expanded and accelerated to rise in the energy storage material. The bubble diameter inside the droplet gradually increased with the increase of rising height until the droplet was completely vaporized. Most of studies on droplet were theoretical, which focused on the volumetric heat transfer coefficient and the temperature distribution along the evaporator. Volumetric heat transfer coefficient, liquid holdup and heat flow rate are important performance parameters of droplets, and they are all functions of temperature. The research showed that the influence of refrigerant flow rate on heat transfer is greater than that of initial refrigerant temperature and PCM temperature [22]. Moreover, the initial drop had an inverse effect on the average volumetric heat transfer coefficient. Nozzle aperture is one of the important parameters for performance prediction and design of direct contact heat exchanger. When the refrigerant droplets injected with its saturation temperature, the optimal refrigeration performance was achieved. The continuous temperature changes of refrigerant droplets during the dynamic movement of heat absorption, vaporization and rise in PCM energy storage materials were simulated and tested experimentally [23-26]. The temperature difference between the interface and the droplets saturation temperature was the driving force to the evaporation. So when the interface temperature of the PCM material was tested, the direct contact evaporator heat transfer coefficient was calculated. But the research results revealed that the calculated valued was different when interface temperature and PCM temperature were adopted in the calculated model, respectively. So, analytical models and experimental test to study the refrigeration system adopted direct contact heat exchanger are very rare for many complex interacting phenomena.

Although the refrigerant direct contact injection refrigeration system has very high refrigeration efficiency, but it also has a very fatal ice blockage problem. As the refrigerant evaporate in PCM material, some water molecules are adsorbed on the refrigerant molecules and sucked back to the compressor. Since the freezing point of water is higher than that of refrigerant, water molecules freeze before refrigerant in the throttling process. As the refrigeration cycle continues, the ice gradually accumulating in the nozzle, which results the ice blockage. Therefore, it also paralyzes the whole refrigeration system. So far, this ice blockage problem has not been completely solved, which hinders the development of direct contact refrigeration system.

Therefore, in order to ensure the continuous external cooling of the refrigeration system, based on the above theoretical analysis and our previous research, the refrigerant direct injection dynamic two-stage refrigeration cycle directly driven by distributed photovoltaic energy system was proposed in this paper. The first stage chiller efficiently produces cold water, part of the cold water is used to cool the high temperature and high pressure vapor refrigerant discharged by the compressor of the second refrigerant direct injection refrigeration system and the surplus cold water is used to service user. Since the two-stage refrigeration systems do not interfere with each other, even if the direct injection refrigeration system stops working due to the ice blockage, the first stage chiller can still operate efficiently to service the user. This working mode has high engineering application value. Firstly, theoretical analysis and experimental test were carried out. The dynamic two-stage high efficiency refrigeration coupling mode combining direct cooling with high evaporation temperature and surplus cold stored with foam slurry ice by liquid-liquid-vapor heat exchanger in the second stage, which effectively solved the problem of the low efficiency of the single static ice making and energy storage system by the efficient coordination of refrigerant cooling and energy storage. At the same time, through the allocation of control strategy, the distributed photovoltaic energy system is effectively combined with the refrigerant direct injection dynamic two-stage refrigeration system to achieve the purposes of ice storage instead of battery to store solar energy.

2. Experiment

2.1. Experimental Setup

Figure 1 shows the schematic of dynamic two-stage refrigerant direct injection refrigeration system directly driven by distributed photovoltaic energy system (DPES). The system is comprised of DPES, the first stage chiller refrigeration cycle, low temperature water cycle and the second stage refrigerant direct injection ice making cycle.

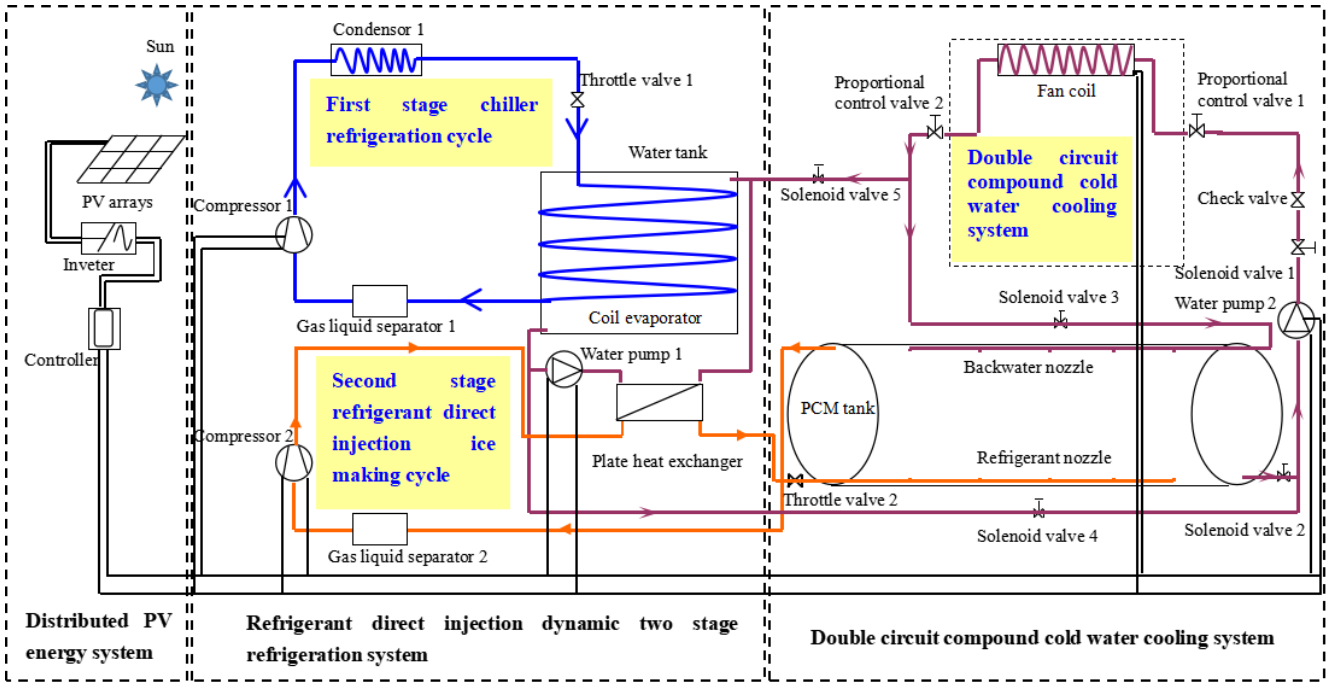

Figure 1. *Schematic diagram of experimental setup.*

DPES is composed of photovoltaic arrays, inverter and controller with maximum power point tracking. The electric energy generated by DPES is used to ensure that compressors, water pumps and other equipment operate efficiently and stably. Moreover, the system energy control strategy and matching coupling control are competed by the intelligent controller. The compressor 1 of chiller operates intermittently to ensure that the temperature of water in the storage tank is maintained at about 5°C ~ 8°C. Water pump pumps the low temperature water stored in the storage tank into the plate heat exchanger to cool the high temperature and high pressure refrigerant discharged by the compressor 2 of the second stage refrigerant direct injection ice making cycle, and then flows back to the water storage tank. In refrigerant direct injection ice making cycle, compressor 2 compresses the refrigerant into high temperature and high pressure gas, which is condensed into low temperature and high pressure gas by the plate heat exchanger and then is throttled into low temperature and low pressure liquid refrigerant. The refrigerant sprays into the PCM material tank through the nozzle arranged at the bottom of the tank. After the refrigerant is sprayed and vaporized in PCM material, it is wrapped by water in gaseous form. At this time, the cooling capacity is directly transferred to the PCM material. In ice making process, the vapor refrigerants are wrapped in the ice grains. Under the action of buoyancy, the ice grains gradually float up to the surface of liquid PCM. When ice grains reach the surface, the gas overflows from the ice and the gaps are left. With the development of refrigeration cycle, a lot of empty ice grains accumulate on the liquid surface of PCM and form foam ice layer. After that, the vapor refrigerant discharged from the ice is sucked back to the compressor 2. This moment, one refrigeration cycle of the second stage refrigeration system is completed. When the refrigerant is directly injected into PCM material, the refrigerant is in direct contact with PCM. The cold capacity of refrigerant is completely absorbed by liquid PCM material. So the refrigeration efficiency is greatly improved. In addition, the injection temperature of refrigerant is about -15°C ~ -5°C, which can effectively alleviate the super-cooling phenomenon and further improve the refrigeration efficiency. So the dynamic two-stage refrigerant direct injection refrigeration system proposed in this paper can effectively solve the disadvantages of low efficiency of traditional static ice making system.

So according to the working principle shown in Figure 1, A 2kW dynamic two-stage refrigerant direct injection refrigeration system directly driven by DPES was constructed and the photos were shown in Figure 2. Moreover, the main component parameters are shown in Table 1.

Table 1. *Component parameters.*

DPES		First stage		Second stage		Cold supply system	
Component	**value**	**Component**	**value**	**Component**	**value**	**Component**	**value**
PV module Max power	245 W	Compressor	1.10 kW	Compressor	0.35 kW	Water pump	0.10 kW
Number of PV module	10	Water tank	125 L	Tank	282 L	Fan coil	0.25 kW
Connection mode	in series	Pipe length	3.5 m	PCM	200 L		
Inverter	220 V3 kW	Total Water	150 L	Water pump	0.15 kW		
Controller	30A load 3 kW	Fan	0.05kW	Capillary length	0.5m		
		Water pump	0.10 kW	Capillary inner diameter	2mm		

2.2. Measurement System

Solar irradiation was measured by pyranometer, wind speed was measured by the wind speed sensor and the ambient temperature was measured by temperature sensor. Moreover, the refrigerant temperatures in two stage refrigeration cycle were measured by T-type thermocouples, shown in Figure 3. Meanwhile, voltages and currents of PV modules were measured by Solar 300N. The compressor operating power was measured by Solar 300N too. Finally, the electromagnetic flow meter was used to measure water flow and refrigerant flow. The parameters, accuracy and measurement uncertainty of all instruments are shown in Table 2.

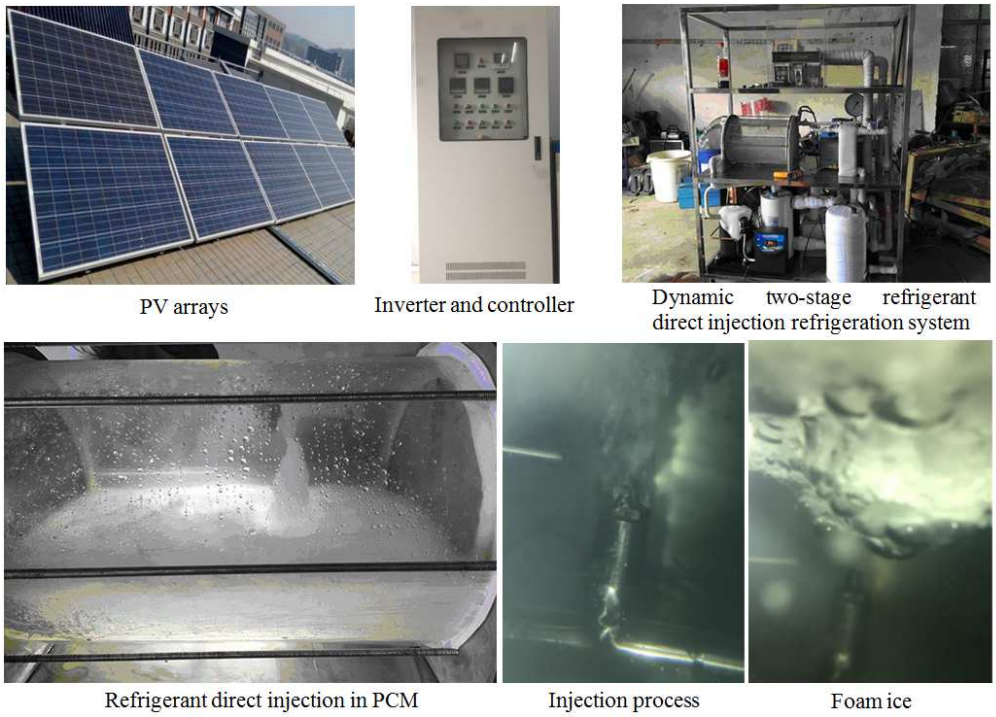

Figure 2. *Experimental platform.*

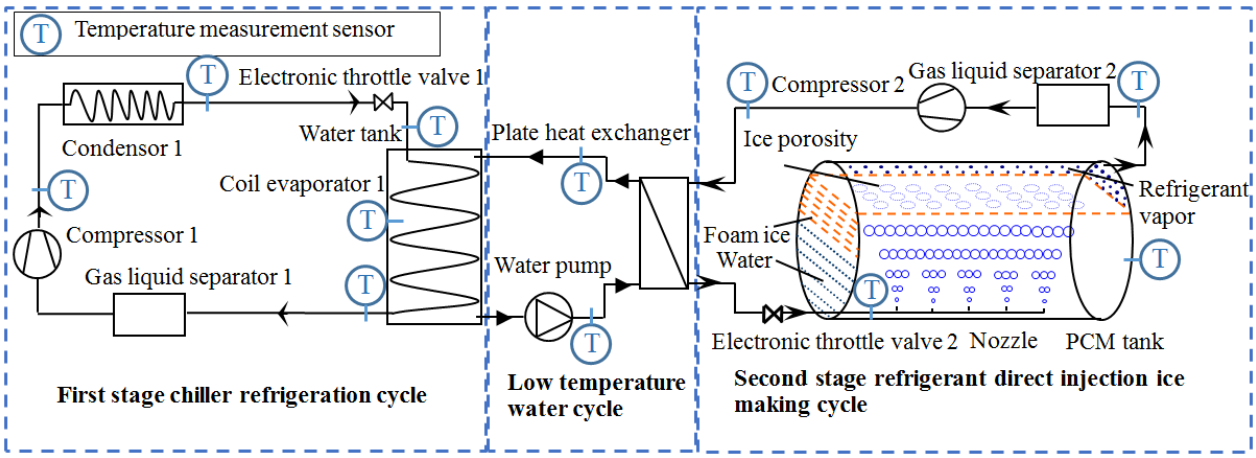

Figure 3. *Thermocouples distribution over the test section.*

Table 2. *Instrument parameters and measurement uncertainty.*

Instrument	Model	Range	Accuracy	Application scope	Maximum relative error	Maximum absolute error	Uncertainty (B class)
Thermocouples	T	-200-350℃	±0.4%	0-150℃	±0.93%	±1.4℃	0.8083
Pyranometer	Kipp&Zonen CMP-6	0-2000W·m^{-2}	±5%	0-1000 W·m^{-2}	±10%	±100 W·m^{-2}	57.7348 W·m^{-2}
Wind speed sensor	EC-9S	0-70 m·s^{-1}	±0.4%	0-10 m·s^{-1}	±2.8%	±0.28 m·s^{-1}	0.1617 m·s^{-1}
Electromagnetic flow meter	KROHNE OPTIFLUX 5000	0-12 m·s^{-1}	±0.15%	0-5 m·s^{-1}	±0.36%	±0.018 m·s^{-1}	0.0104 m·s^{-1}
Digital multimeter	Solar 300N	Voltage: 0-1000 V Current: 0-10 A	±0.9% ±1%	0-380 V 0-10 A	±2.37% ±1%	±9.006 V ±0.1 A	5.1996 V 0.0577 A
Electronic balance	AHW-3	0-3kg	±0.05g	0-3kg	±0.05%	±0.0015 kg	0.0009 kg

3. Modelling

3.1. Energy Transfer Process of DPES

The transient energy balance equation of PV arrays [27]:

$$(m\mathrm{Cp}_{module})\frac{dT_p}{dt} = Q_{pv,in} - Q_{pv,rad} - Q_{pv,conv} - Q_{pv,elect} \quad (1)$$

Where, mCp_{module} is photovoltaic module heat capacity, kJ/K. T_p is PV module temperature, K. $Q_{pv,in}$ is solar irradiance power obtained by PV arrays, kW. $Q_{pv,rad}$ is radiation power loss, kW. $Q_{pv,conv}$ is convective heat loss power, kW. $Q_{pv,elect}$ is electric power converted by PV arrays, kW.

The solar energy collected by PV arrays is calculated by:

$$Q_{pv,in} = \tau G S_p \quad (2)$$

Here, τ is the product of PV module cover glass transmittance and PV cell surface absorptivity, experimental value is 0.75. G is solar irradiance accepted by PV arrays, W/m^2. S_p is PV module area, m^2.

The calculation formula of radiant heat loss is given by:

$$Q_{pv,rad} = Q_{pv,rad-ground} + Q_{pv,rad-sky} \quad (3)$$

$$Q_{pv,rad-ground} = S_p F_{pg} \sigma \left(\varepsilon_p T_p^4 - \varepsilon_g T_g^4\right) \quad (4)$$

$$Q_{pv,rad-sky} = S_p F_{ps} \sigma \left(\varepsilon_p T_p^4 - \varepsilon_s T_s^4\right) \quad (5)$$

$Q_{pv,rad\text{-}ground}$ is ground radiation heat loss of PV arrays, W, which can be ignored when PV arrays are installed in unobstructed areas. $Q_{pv,rad\text{-}sky}$ is the radiation heat loss of PV arrays to sky, W. σ is Stephan-Boltzmann constant, 5.76×10^{-8} W/(m^2·K^4). F_{ps} is transparency factor of PV arrays to sky, 1. ε_p is PV arrays average emissivity, 0.88. ε_g is average ground emissivity and ε_s is average sky emissivity, 1. T_g and T_s are ground temperature and sky temperature, respectively. Generally, the sky temperature is 0.914 times of the ambient temperature [28].

The calculation formula of heat loss of surface convective heat transfer is given by:

$$Q_{pv,conv} = S_p H \left(T_p - T_a\right) \quad (6)$$

Here, H is convective heat transfer coefficient between PV arrays and air, W/(m^2·K), which can be calculated by the follow empirical formula [29].

$$H = 1.2475\left[\Delta T \cos\beta\right]^{1/3} + 2.686 V_{wind} \quad (7)$$

ΔT is different temperature between PV modules and ambient, K. β is PV arrays installation angle and the tested value is 25°. V_{wind} is wind speed during test, m/s.

The generating power by PV arrays is given by:

$$Q_{pv,elect} = \eta G S_c \quad (8)$$

η is photoelectric conversion efficiency. S_c is PV cells total area, m^2.

$$\eta = \eta_0 \left[1 - \gamma\left(T_p - T_r\right)\right] \quad (9)$$

Where, η_0 is photoelectric conversion efficiency under standard conditions, 17.5%. γ is temperature transfer factor of photoelectric conversion efficiency, 0.0042K^{-1}; T_r is reference temperature, 298 K. In this paper, the output efficiency of the integrated reverse and control machine is about 92%.

3.2. Energy Transfer Process of the First Stage Chiller Refrigeration Cycle

The compressor energy balance equation is given by:

$$Q_{CP,in} + W_{p,1} = Q_{CP,out} + Q_{CP,loss} \quad (10)$$

$Q_{CP,in}$ is input compressor energy per unit time, W. $Q_{CP,out}$ is compressor output energy per unit time, W; W_p is compressor input power, W; $Q_{CP,loss}$ is compressor energy loss per unit time, W. generally, it is taken as 10% of compressor operating power.

State 1 is dry vapor with saturation temperature. And the refrigerant state parameters are obtained from the refrigerant saturation properties table. The energy balance equations in the steam compression refrigeration system are shown as follows:

$$Q_{CP,in/out} = \dot{m}_{rf,1} h_{1/2,1} \quad (11)$$

$$Q_{CO,in} = Q_{CO,out} + Q_E \quad (12)$$

$Q_{CO,in}$ is condenser input energy per unit time, W. $Q_{CO,out}$ is condenser output energy per unit time, W. Q_E is condenser discharging heat to outside per unit time, W.

$$Q_{CO,in} = Q_{CP,out} \tag{13}$$

$$Q_E = \dot{m}_{air,con} C_{P,air} \left(t_{air,out} - t_{air,in} \right) \tag{14}$$

$$Q_{TH,in} = Q_{TH,out} \tag{15}$$

$$Q_{TH,in} = Q_{CO,out} \tag{16}$$

$Q_{TH,in}$ is throttle input energy per unit time, W; $Q_{TH,out}$ is throttle output energy per unit time, W.

The energy balance equation of evaporator is shown as:

$$Q_{EV,in} + Q_{AB} = Q_{EV,out} \tag{17}$$

$$Q_{EV,in} = Q_{TH,out} \tag{18}$$

$$Q_{EV,out} = Q_{CP,in} \tag{19}$$

At the time n, the energy balance inside the evaporator of the first stage chiller refrigeration cycle is given by:

$$Q^n_{EV,in} + Q^n_{AB} = Q^n_{EV,out} \tag{20}$$

$$Q^n_{EV,in} = Q^{n\text{-}1}_{EV,out} + 0.9W^n_1 \tag{21}$$

$$Q^n_{AB} = Q^{n\text{-}1}_{EV,out} - Q^n_{EV,out} + 0.9W^n_{p,1} - Q_E \tag{22}$$

$$Q^n_{EV,out} = \dot{m}^n_{1,1} h^n_{1,1} \tag{23}$$

$$Q^n_{AB} = \dot{m}_{rf,1} \left(\frac{W^{n-1}_{p,1}}{W_{p,1}} \right) h^{n-1}_{1,1} - \dot{m}_{rf,1} \left(\frac{W^n_{p,1}}{W_{p,1}} \right) h^n_{1,1} + 0.9W^n_{p,1} - Q_E \tag{24}$$

$$h^n_{1,1}\left(t_1\right) = 0.6143t_1 + 398.05 \tag{25}$$

The cooling capacity produced by the evaporator at the n time can be obtained by:

$$Q^n_{AB} = \frac{\dot{m}_{rf,1}}{W_{p,1}} \left[0.6143 \left(W^{n-1}_{p,1} t^{n-1}_{1,1} - W^n_{p,1} t^n_{1,1} \right) + 398.05 \left(W^{n-1}_{p,1} - W^n_{p,1} \right) \right] \cdot 10^3 + 0.9W^n_{p,1} - \dot{m}_{air,con} C_{P,air} \left(t^n_{air,out} - t^n_{air,in} \right) \tag{26}$$

The cumulative refrigerating capacity of the first stage refrigeration system is shown by:

$$Q_{AB} = \sum_1^t Q^n_{AB} \tag{27}$$

3.3. Energy Transfer Process of the Second Stage Refrigerant Direct Injection Refrigeration Cycle [30]

3.3.1. Plate Heat Exchanger

The calculation formula of instantaneous energy obtained by the secondary refrigeration system from the first stage refrigeration system is given by:

$$Q^n_{2,con} = kA \left(\frac{t^n_{3,2} + t^n_{4,2}}{2} - \frac{t^n_{ex,in} + t^n_{ex,out}}{2} \right) \tag{28}$$

$t^n_{3,2}$, $t^n_{4,2}$, $t^n_{ex,in}$ and $t^n_{ex,out}$ are respectively compressor discharge temperature, refrigerant temperature flowing out of plate heat exchanger, the inlet temperature of the first stage refrigeration system to plate heat exchanger and the outlet temperature of the first stage refrigeration system to plate heat exchanger in the secondary refrigeration system,°C. k is the total heat transfer coefficient of plate heat exchanger, $W \cdot m^{-2} \cdot °C^{-1}$. A is the heat exchange area of plate heat exchanger, 1.4 m^2.

The total heat transfer coefficient k of plate heat exchanger can be calculated by the following formula:

$$\frac{1}{k} = \frac{1}{\alpha_h} + \frac{1}{\alpha_c} + \frac{\delta}{\lambda} + R_1 + R_2 \tag{29}$$

Where, α_h and α_c are convective heat transfer coefficients of cooling side and receiving cold side of plate heat exchanger respectively, $W \cdot m^{-2} \cdot °C^{-1}$. δ is plate heat exchanger plate thickness, m, λ is plate thermal conductivity, $W \cdot m^{-1} \cdot °C^{-1}$. R_1 and R_2 are the fouling coefficient of cooling side and receiving cold side respectively, 0.000030 and 0.000172. At this moment, α_h and α_c can be given by:

$$\alpha_h = \frac{\lambda_h}{de_h} Nu_h \tag{30}$$

$$\alpha_c = \frac{\lambda_c}{de_c} Nu_c \tag{31}$$

Here, de_h is plate diameter, which is twice of the plate spacing, m. Nu_h and Nu_c are the Nushilt numbers of cooling side and receiving cold side of plate heat exchanger respectively.

Because the equal flow channel is adopted in the plate heat exchanger, so the Nushilt numbers are calculated as follows:

$$Nu_h = 0.308 \, \mathrm{Re}_h^{\,0.6376} \, \mathrm{Pr}_h^{\,0.3} \tag{32}$$

$$Nu_c = 0.308 \, \mathrm{Re}_c^{\,0.6376} \, \mathrm{Pr}_h^{\,0.4} \tag{33}$$

Where, Re_h and Re_c are the Reynolds numbers of the cooling side and receiving cold side, respectively. Pr_h and Pr_c are the Prandtl numbers of the cooling side and receiving cold side, respectively. All of the Reynolds and Prandtl numbers can be obtained by looking up the relevant reference Tables.

3.3.2. Capillary Restrictor

The mass flow of refrigerant flowing out of capillary tube, which was also the mass flow of working medium direct injection, can be calculated by the following empirical formula:

$$\dot{m}_2 = \mathrm{C}_1 d^{C_2} L^{C_3} T^{C_4}_{4,2} 10^{C_5 T_{sc}} \tag{34}$$

Here, C_1, C_2, C_3, C_4 and C_5 are empirical constants, shown in Table 3.

Table 3. *Empirical constants.*

Refrigerant	C_1	C_2	C_3	C_4	C_5
R22	0.249029	2.543633	-0.42753	0.746108	0.013922
R134a	0.123237	2.498028	-0.41259	0.840660	0.018751
R407C	0.246647	2.544032	-0.41953	0.755385	0.013678
R410A	0.406125	2.589643	-0.45475	0.696669	0.011865

t_{sc} is the super-cooling degree of the refrigerant, which can be calculated as follows:

$$t_{sc} = t_{4sc,2} - t_{4,2} \tag{35}$$

$t_{4sc,\ 2}$ is the temperature of the saturated liquid refrigerant corresponding to $P_{4,\ 2}$, which can be obtained by referring to the table.

Here,

$$P_{4,2} = 303.73e^{0.0305t_{4\ ,\ 2}} \tag{36}$$

$$t_{4sc,2} = 28.008 \ln P_{4,2} - 181.36 \tag{37}$$

The empirical formula for capillary length calculation is given by:

$$L = \frac{\Delta P \cdot \mathrm{Re}^{0.25} \cdot d_2 \cdot 2g}{0.3164 \cdot v_{rf,2}{}^2 \cdot \rho} \tag{38}$$

Where, ΔP is the pressure difference between the inlet and outlet of the capillary, therefore:

$$\Delta P = P_{4,2} - P_{5,2} \tag{39}$$

Thus, the nozzle injection pressure $P_{5,2}$ is shown as:

$$P_{5,2} = P_{4,2} - \frac{3.1 \cdot 10^{-3}}{\mathrm{Re}^{0.25}} \cdot \frac{L}{d_2} \cdot \frac{v_{rf,2}{}^2}{2g} \cdot \rho \tag{40}$$

$P_{4,2}$ and $P_{5,2}$ are expressed with kPa.

At this time, the nozzle temperature $t_{2,5}$ can be calculated by the following empirical formula:

$$t_{5,2} = 0.0958 P_{5,2} - 52.096 \tag{41}$$

3.3.3. Refrigerant Injection Refrigeration Process

Firstly, the heat transfer process of a single bubble is studied. The average heat transfer coefficient per unit area of a single bubble surface is shown as follow:

$$h = \sqrt{\frac{2U}{\pi \alpha R}} \lambda_c \tag{42}$$

R is the equivalent spherical radius of two-phase bubbles of diffusion phase (refrigerant), m. λ_c is continuous phase (PCM material) thermal conductivity, $\mathrm{W \cdot m^{-1} \cdot °C^{-1}}$. U is the rising velocity of two-phase bubble, $\mathrm{m \cdot s^{-1}}$. α is continuous phase liquid thermal diffusivity, $\mathrm{m^2 \cdot s^{-1}}$.

The Nusselt number of single bubble heat transfer is given by:

$$Nu = \frac{2hR}{\lambda_c} = \frac{2}{\sqrt{\pi}} (Pe)^{1/2} \tag{43}$$

P_e is the Beckley criterion number (Pe=Re*Pr), 28000.

3.3.4. Two Phase Bubble Growth Process

Assuming that there is no aggregation and rupture of bubbles in rising process. This moment, the mass in the spherical boundary is conserved. The energy balance equation is shown as:

$$m + \rho_v \left(\frac{4}{3} \pi R^3 - \frac{m}{\rho_l} \right) = m_0 \tag{44}$$

m_0 and m are the initial mass and residual liquid mass of two-phase bubbles respectively, kg. ρ_v and ρ_l are the gas phase density and liquid phase density in two-phase bubbles respectively, $\mathrm{kg \cdot m^{-3}}$.

$$\left(\frac{\rho_v}{\rho_l} - 1 \right) \frac{dm}{d\tau} = \rho_v 4\pi R^2 \frac{dR}{d\tau} \tag{45}$$

Because $\rho_v << \rho_l$, Therefore:

$$-\frac{dm}{d\tau} = \rho_v 4\pi R^2 \frac{dR}{d\tau} \tag{46}$$

According to the law of conservation of energy.

$$-h_{fg} \frac{dm}{d\tau} = 4\pi R^2 h (t_c - t_i) \tag{47}$$

Where, h_{fg} is dispersed phase liquid evaporation latent heat, J/kg, t_c is the main body temperature of continuous phase,°C. t_i is the two-phase interface temperature,°C.

The calculation formula of bubble growth rate is shown as:

$$\frac{dR}{d\tau} = \frac{h}{\rho_v f_{hg}} (t_c - t_i) = \frac{\alpha}{2R} \mathrm{Nu} J_\alpha \tag{48}$$

Where, $Nu=2hR/\lambda_c$, Jα is Jacobian criterion number. $\alpha=\lambda_c/\rho l\mathrm{Cp}$, Cp is specific heat capacity of continuous phase liquid, $\mathrm{kJ \cdot kg^{-1} °C^{-1}}$.

$$J_\alpha = \frac{\rho_l C_p}{\rho_v h_{h,g}} (t_c - t_i) \tag{49}$$

$$\frac{R}{R_0} = \left(1 + \frac{3J_\alpha \tau}{2R_0^{3/2}} \sqrt{\frac{2U\alpha}{\pi}} \right)^{2/3} \tag{50}$$

R_0 is initial radius of two phase bubble, 0.0006m.

Therefore, the heat transfer coefficient formula of a single bubble can be summarized as follows:

$$h=\lambda_c\sqrt{\frac{2U}{\pi\alpha}}\left(R_0^{3/2}+\frac{3J_\alpha\tau}{2}\sqrt{\frac{2U\alpha}{\pi}}\right)^{-1/3} \tag{51}$$

Nusselt number is given by:

$$N_u=2\sqrt{\frac{2U}{\pi\alpha}}\left(R_0^{3/2}+\frac{3J_\alpha\tau}{2}\sqrt{\frac{2U\alpha}{\pi}}\right)^{1/3} \tag{52}$$

Assuming that the droplet just reaches the surface of the liquid column when it is completely evaporated. At this moment, the mass conservation of the droplet is as follows:

$$\frac{4}{3}\pi R_0^{\ 3}\rho_l=\frac{4}{3}\pi R_f^{\ 3}\rho_v \tag{53}$$

$$R_f=\left(\frac{\rho_l}{\rho_v}\right)^{1/3}R_0 \tag{54}$$

R_f is the bubble radius when the droplet evaporates completely, m. The droplet radius R_0 can be calculated by the following formula:

$$R_0=Cv^{0.35}d_h^{0.72} \tag{55}$$

v is the jet velocity at the nozzle, $m\cdot s^{-1}$. d_h is the nozzle diameter, m. C is the empirical constant, 0.1535. According to the above formula, the time required for complete evaporation of droplets is calculated by:

$$\tau_f=\frac{2}{3}\frac{R_0^{3/2}}{J_\alpha}\left[\left(\frac{\rho_l}{\rho_v}\right)^{1/2}-1\right]\sqrt{\frac{\pi}{2U\alpha}} \tag{56}$$

The number of bubbles generated by the secondary refrigeration system per unit time is calculated by:

$$n=\frac{Q_v}{\frac{4}{3}\pi R_0^{\ 3}} \tag{57}$$

Where, Q_v is the volume flow of refrigerant before injection into the tank, $m^3\cdot h^{-1}$.

The total number of bubbles in the tank is given by:

$$n_v=n\tau_f=\frac{Q_v}{\frac{4}{3}\pi R_0^{\ 3}}\cdot\tau_f \tag{58}$$

The instantaneous volume heat transfer coefficient in the tank is shown as follow:

$$h_{vin}=n_v 4\pi R^2 h=\frac{Q_v\tau_f}{\frac{4}{3}\pi R_0}\cdot 4\pi R^2\cdot\sqrt{\frac{2U}{\pi\alpha R}}\lambda_c =\frac{2Q_v\lambda_c R_0^{3/2}}{\alpha\cdot J_\alpha}R^{3/2} \tag{59}$$

$$R^{3/2}=R_0^{3/2}+\frac{3}{2}\sqrt{\frac{2\alpha}{\pi U}}J_\alpha Z \tag{60}$$

$$h_{vin}=\frac{2Q_v\lambda_c R_0^{3/2}}{\alpha\cdot J_\alpha}\left(R_0^{3/2}+\frac{3}{2}\sqrt{\frac{2\alpha}{\pi U}}J_\alpha Z\right) \tag{61}$$

The average heat transfer coefficient of bubbles in the tank is given by:

$$h_v=\frac{2Q_v\lambda_c R_0^{3/2}}{\alpha\cdot J_\alpha}\left(R_0^{3/2}+\frac{3}{4}\sqrt{\frac{2\alpha}{\pi U}}J_\alpha H\right) \tag{62}$$

4. Results and Discussion

4.1. Model Validation

Based on the measured climate conditions, shown in Figure 4a, the power generation of DPES and the coefficient of performance (COP) of two stages refrigeration system were simulated by the formulas described above. After that, the experimental test was carried out with the experimental test platform. All of the experimental data were compared with the calculation results, shown in Figure 4b.

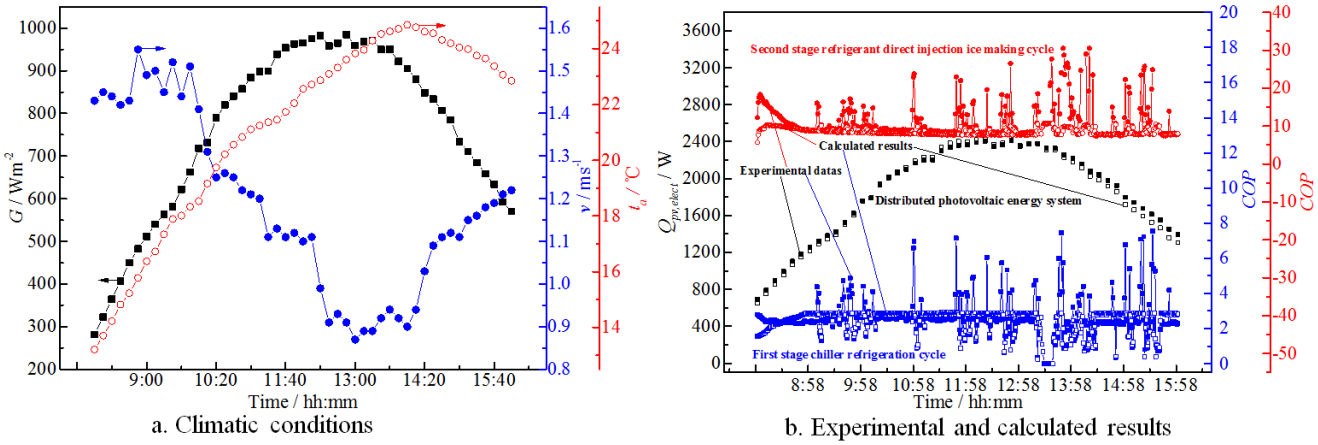

a. Climatic conditions b. Experimental and calculated results

Figure 4. *Model validation.*

In Figure 4a, it was obvious that the experiment was carried out in a typical sunny day from 8:00 A.M to 4 P.M. The cumulative irradiation amount and average solar irradiance during the experiment were 21.34 MJ/m^2 and 760.78W/m^2, respectively. In addition, the average wind speed and ambient temperature were 1.18 m/s and 21.14°C, respectively. And the average photoelectric conversion efficiency of PV arrays was 17.99%. It could be seen from Figure 4b that the calculated values of the instantaneous generation power of DPES and the instantaneous COP of the two refrigeration cycles were in good agreement with the experimental data. The relative errors were shown in Table 4. It was obvious that the relative error of the refrigerant direct injection refrigeration cycle was more than 10%, because the refrigerant direct contact heat transfer process was very complex. There was no mature theoretical model at present. So more empirical formulas were used in the calculation process. Therefore, the accumulation of empirical formula errors leaded to the increase of the final calculation errors. However, this error was acceptable in the engineering field. So it could be concluded that the model reported in the paper was reliable and practical, which could be used to calculate the performance of dynamic two-stage refrigerant direct injection refrigeration system directly driven by DPES.

Table 4. *Relative errors of calculated values (R410a).*

	DPES	**First stage chiller refrigeration cycle**	**Second stage refrigerant direct injection refrigeration cycle**
	Accumulated power / kW•h	**Average COP**	**Average COP**
Calculated values	15.066	2.607	9.557
Experimental data	15.222	2.479	8.523
Relative errors	-1.03%	5.16%	12.13%

4.2. Refrigeration Performance

The refrigeration performances of three refrigerants such as R22, R134a and R318, which were employed in two-stage refrigerant direct injection high efficiency refrigeration system driven by power grid, were investigated by experiment. Moreover, the temperatures of components in the refrigeration system were measured and recorded. The results were showed in Figure 5a, Figure 5b and Figure 5c.

The experimental results showed that the refrigerant injection refrigerant system could operate stably and efficiently when R22, R134a and R318 were employed as the dispersant in direct contact heat exchanger. Because the first stage chiller was a closed refrigeration cycle, the replacement of refrigerant in the secondary refrigeration system had little effect on its refrigeration performance and its COP was basically maintained at about 3. In the second stage refrigeration cycle, the average COPs of injection refrigeration system with R22, R134a and R318 refrigerant were 6.16, 5.80 and 8.70, respectively. After the same capillary throttling, R22 temperature at the nozzle could reach -17.29°C, which was the lowest temperature in three refrigerants. The minimum temperatures of R134a and R318 at the nozzle were -10.02°C and -5.09°C, respectively.

Table 5 showed that the main research results and was close to those of Kiatsirriroat et al [19, 30], Sidemen [31] and Blair [32]. It was obvious that the volumetric heat transfer coefficient of refrigerant droplets h_v of R22 and R134a in this paper were similar to results of Kiatsirriroat. But the COP of R22 of present study was 35.25% higher than reported by Kiatsirriroat. Because the injection temperature of throttled refrigerant at the nozzle was 7.71°C higher than Kiatsirriroat by optimizing the length and inner diameter of capillary.

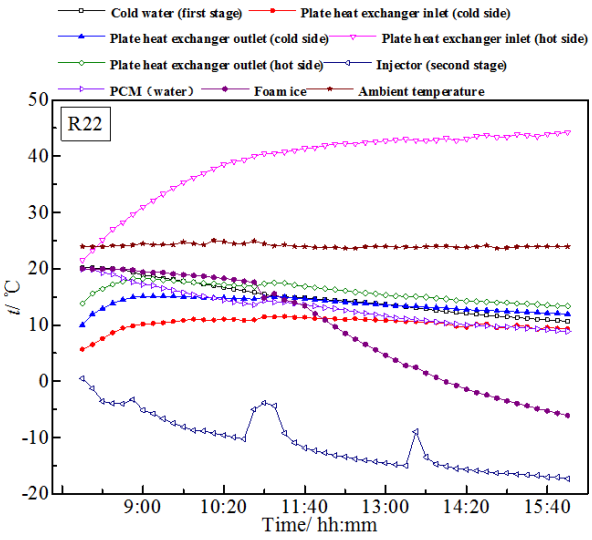

a. Refrigeration performance of R22

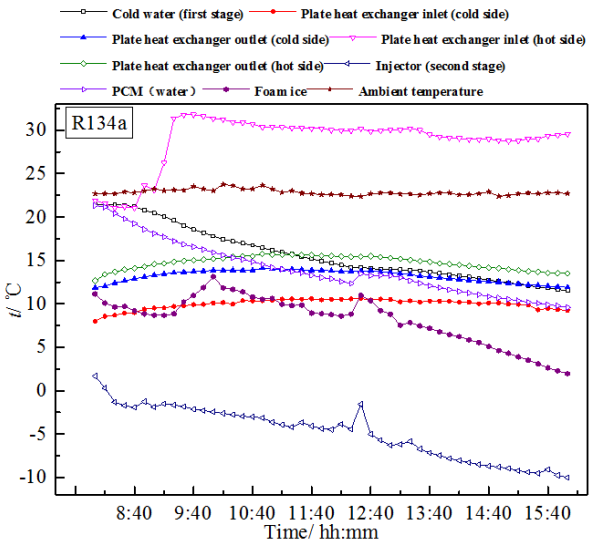

b. Refrigeration performance of R134a

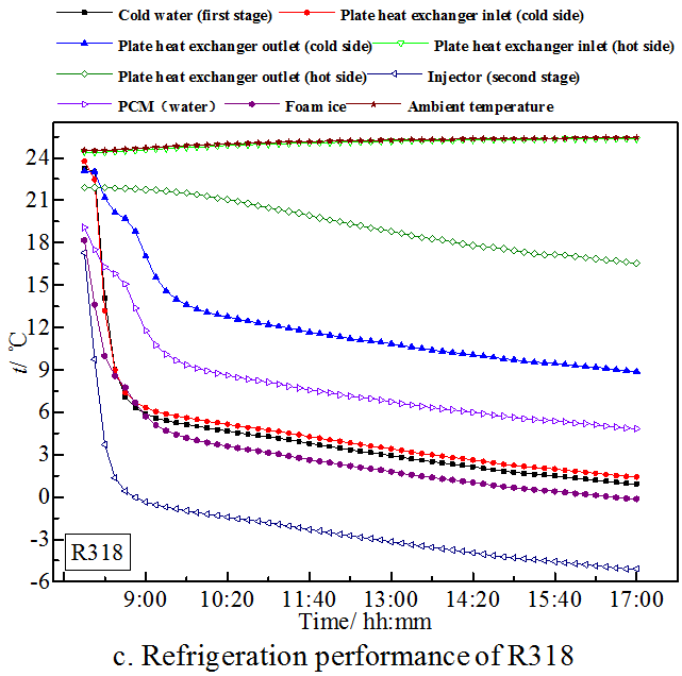

Figure 5. *Refrigeration characteristic curves of the two-stage refrigeration system with three refrigerants.*

Table 5. *Comparison of research results.*

	Present research (Average value)					**Kiatsiriroat [19, 30]**	**Sideman [31]**	**Blair [32]**
Refrigerant	R134a	R22	R407C	R410a	R318	R134a, R12, R22	Pentane	R113
PCM materials	Water	Water	Water	Water	Water	Water	Water	Water
h_v (kW/m^3℃)	39.75	40.62	46.90	65.02	82.27	2-40, 2-16, 2-52	180	122
Mass flow rate of refrigerant (kg/s)	0.008	0.01	0.01	0.01	0.013	0.02-0.08	0.022	0.023
Refrigerant temperature (℃)	-10.02	-17.29	-3.10	-11.28	-5.09	-10.00, -20.00, -25.00	-	-
COP	4.52	5.56	6.13	8.52	8.70	-, -, 3.4-3.6	-	-

In PCM storage tank, the direct contact heat transfer process between refrigerant and PCM material was complex and difficult to test experimentally. Therefore, the heat transfer process and performance of the second stage refrigerant direct injection refrigeration system direct driven by DPES were investigated by calculation. Driven by compressor, the throttled refrigerant droplets were injected into the PCM storage tank. After absorbing the heat energy of PCM material with relatively high temperature, the low temperature droplets gradually vaporized into gaseous refrigerant to form the bubbles in PCM. Under the joint action of injection speed and buoyancy, the refrigerant bubbles floated up to the surface of liquid PCM and then broken. And then, the vapor refrigerant in the bubbles were sucked back to compressor and this moment a refrigeration was completed. With the development of refrigeration cycle, foam ice was gradually formed on the surface of PCM liquid. In this process, the injection speed of refrigerant and the size of nozzle inner diameter had a great impact on the droplet vaporization and bubble rupture height. In addition, the temperature and pressure of throttled refrigerant had a certain impact on the bubbles` motion characteristics. The calculated results were shown in Figure 6.

Figure 6a showed the capillary outlet pressure and temperature curves, which decreased gradually with the increase of time until they reached stability. The curves fluctuated with the fluctuation of solar irradiance. So The average values of pressure and temperature could better evaluate the capillary outlet characteristics and the average values were 436.05 kPa and -11.17°C, respectively. Figure 6b described the refrigerant injection speed, droplets evaporation time, maximum droplet radius and maximum rising height. The injection speed and droplets evaporation time decreased along with the increase of time. On the contrary, the maximum droplet radius and maximum rising height increased along with time. Their average values were 3.89 m/s, 3.58 mm, 0.00164 s and 6.4 mm, respectively. The heat transfer coefficient of refrigerant bubble in PCM material was an increasing function of time, which reached the equilibrium after a certain time, shown in Figure 6c. But the bubble heat transfer power and the number of the bubbles always about kept the same. Their average values were 112, 21.09 W and 12.54 kW/(m^2·K), respectively. Finally, the COPs of the refrigeration system were shown in Figure 6d.

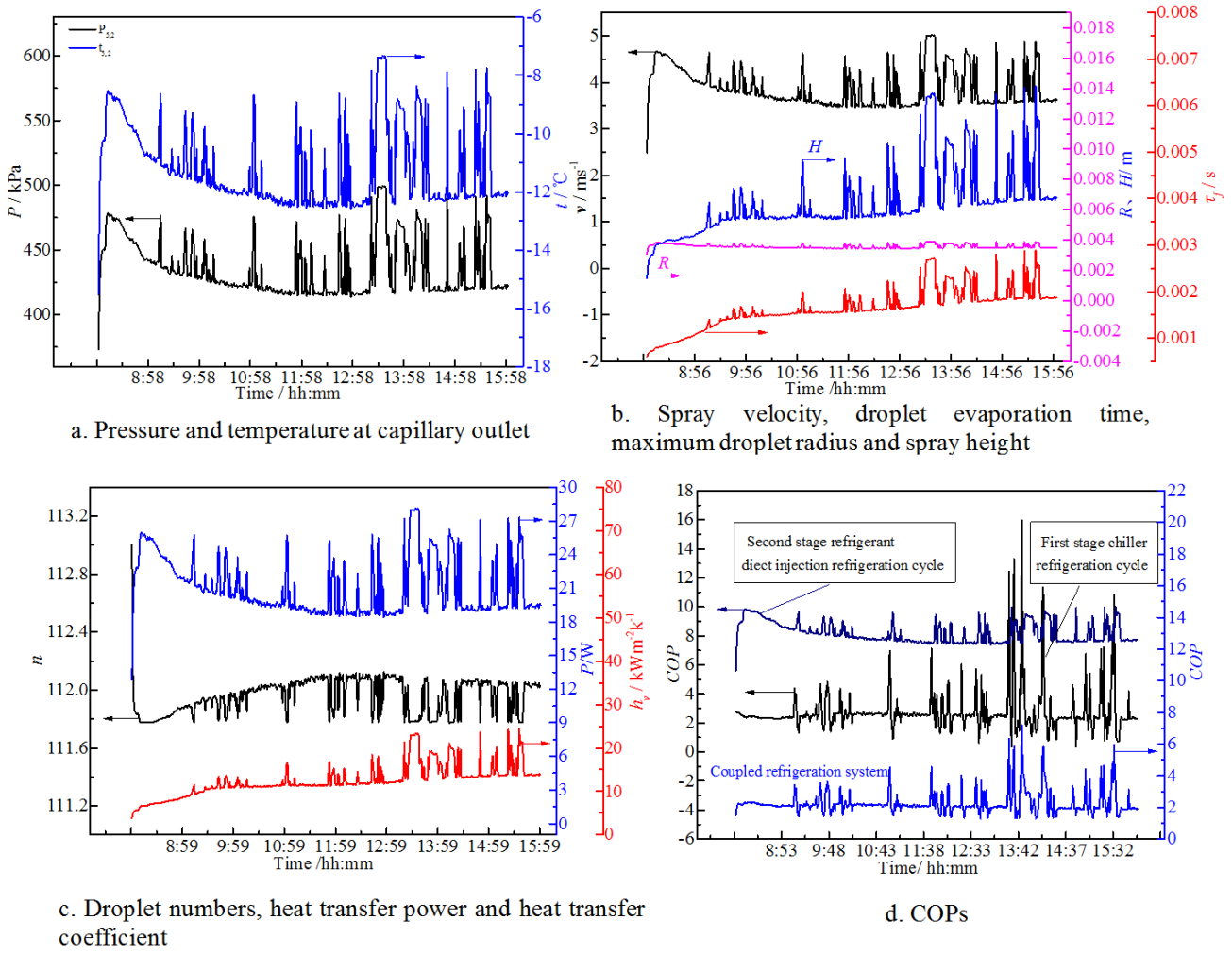

Figure 6. *Refrigerant direct injection characteristics.*

4.3. Influence of Component Parameters on Refrigeration Performance

In the second stage refrigerant direct injection refrigeration system, the plate heat exchanger played a very important role. The cold side of the exchanger was pumped the cold water produced in by the first stage chiller, which was employed to cool the high temperature and pressure vapor refrigerant in the hot side of exchanger. So the exchanger played the role of condenser in the second stage refrigerant. Different from the ordinary air cooled condenser, the water cooled plate heat exchange condenser with better condensation effect was adopted. So the heat transfer effect of plate heat exchanger had a great influence on the characteristics of the condensed refrigerant in the second refrigeration cycle. Therefore, the parameters of plate heat exchanger such as material, wall thickness and heat exchange area, affecting the heat exchange effect of the exchanger were analyzed in this paper. And the research results were shown in Figure 7.

In Figure 7a, it was obvious that with the increase of plate exchanger wall thickness, the average plate total heat transfer coefficient and the COP of the second injection refrigeration cycle of the exchanger gradually decreased. At the same time, the average surplus cooling capacity produced by the first chiller gradually increased. When the wall thickness of plate increased 1mm, the transfer coefficient and COP decreased by 0.234 kW/(m^2°C) and 0.017, respectively and the surplus cooling capacity increased by 0.352 kW. Therefore, the thinner plate was employed, the heat transfer coefficient was greater and more cooling capacity produced by the chiller was transmitted to the second injection refrigeration cycle. So the COP of second stage refrigeration system was improved effectively. Figure 7b showed that the COP of second stage refrigeration system increased along with the increase of thermal conductivity. But the increase rate was gradually decreasing. As you know, the more purchase money must be paid for the better conductivity coefficient plate exchanger. So the plate heat exchangers with large market share usually use materials with medium thermal conductivity and low price, such as cast iron and lead-zinc. Figure 7c revealed that the surplus cooling capacity increased along with the increase of exchanger heat exchange area at an increase rate of -9.39 kW/m^2. Moreover, the COP and the mass flow of the second refrigerant injection refrigeration increased along with the increase of area at the increase rates of 12.92 m^{-2} and 0.0209 kg/(s·m^2), respectively.

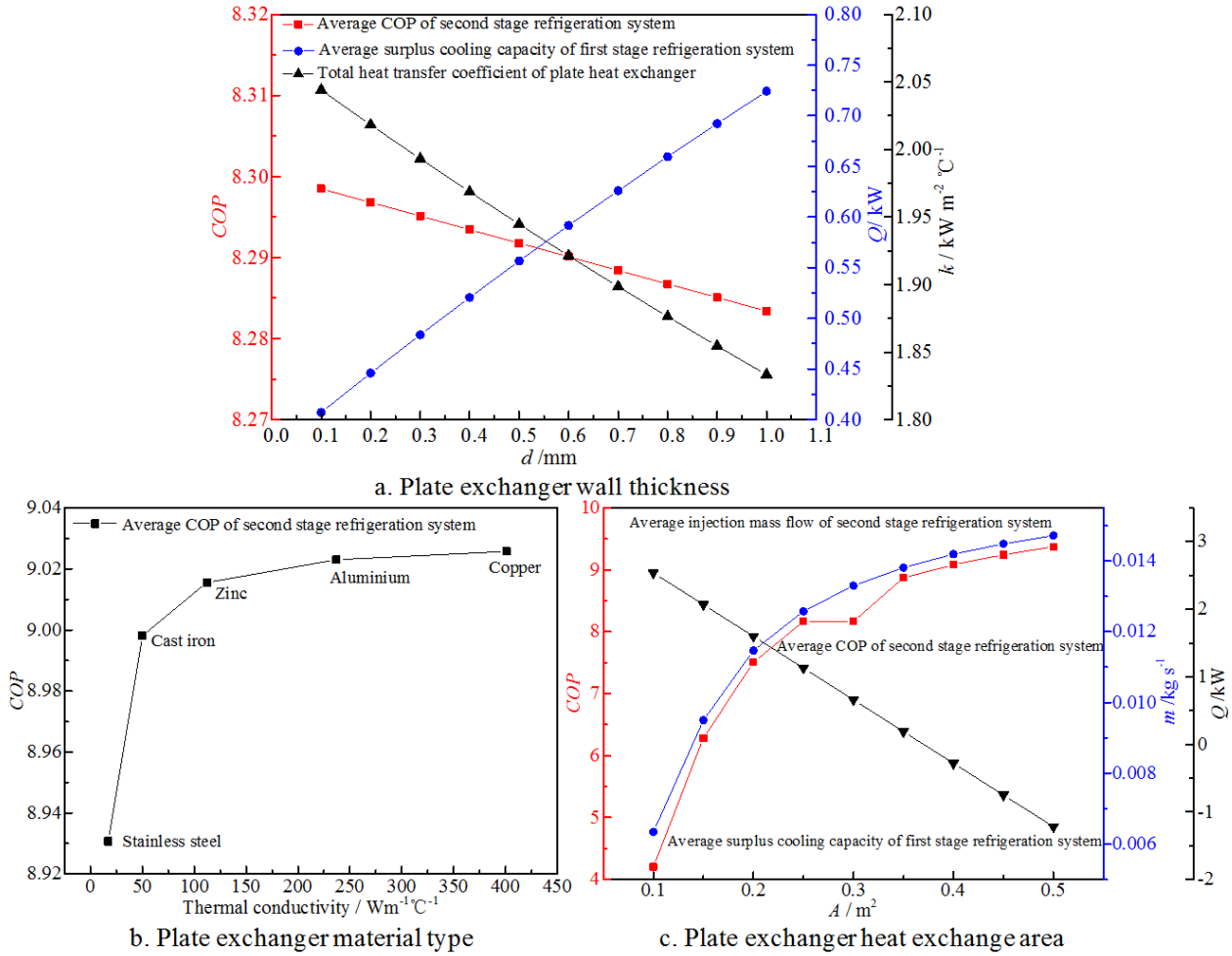

Figure 7. *Effect of heat exchanger parameters on direct injection refrigeration performance of two stage refrigerant direct injection refrigeration system.*

In refrigeration cycle, the saturated or super-cooled low temperature and high pressure refrigerant flowing out of the condenser must be throttled, depressurized and cooled by throttle valve or capillary before the liquid refrigerant can reach saturation again and a refrigeration is finished by liquid endothermic evaporation. In order to investigated the effect of throttling on the refrigeration performance. The capillary was employed in the second stage refrigerant injection refrigeration and the influence of capillary inner diameter and length on the refrigeration characteristics was studied. And the investigated results were shown in Figure 8.

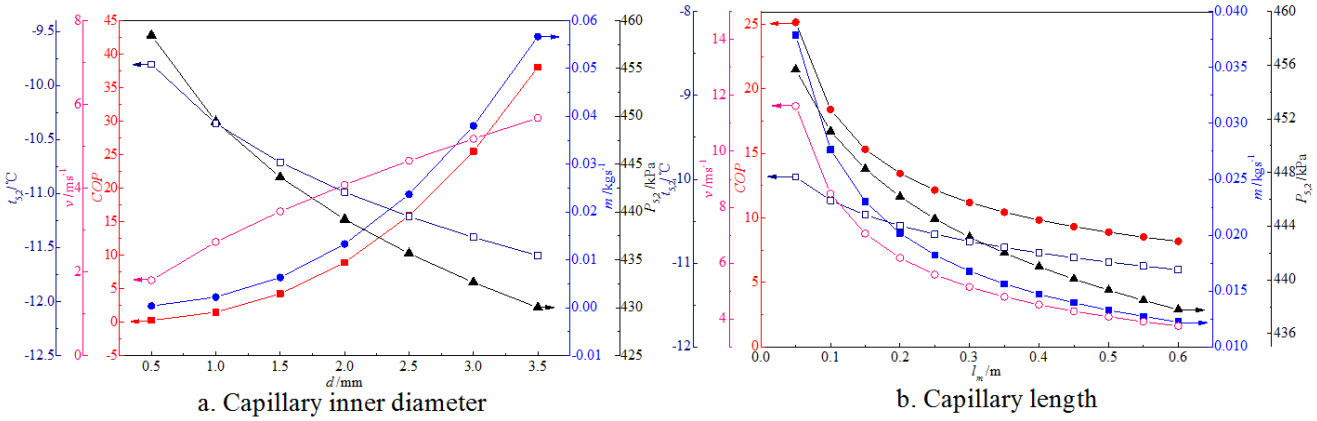

Figure 8. *Effect of capillary parameters on refrigeration characteristics of the second refrigerant injection refrigeration cycle.*

In Figure 8a, the results showed that capillary inner diameter had a complex effect on the refrigeration

characteristics of the second refrigerant injection refrigeration cycle. When the inner diameter d increased, the first effected parameter was capillary outlet refrigerant pressure $P_{5,2}$, which decreased gradually with a -9.484 kPa/mm average increase rate. In throttling process of refrigeration cycle, refrigerant temperature $t_{5,2}$ decreases along with the decrease of the pressure. So the outlet refrigerant temperature also decreased along with the diameter increase at a -0.590°C/mm average increase rate. The refrigerant mass flow and jet velocity of capillary outlet, the COP of the second refrigeration were increased along with the increase of the diameter at the average increase rates of -0.0188 kg/(s·mm), 1.291 m/(s·mm) and 12.597 mm^{-1}. The increase rate of jet velocity decreased gradually. But the increase rates of mass flow and COP increased gradually. In Figure 8b, it was obvious that when capillary length increased, all of the refrigeration characteristics parameters decreased gradually. Because the capillary was extended, the throttling process also increased. So the outlet pressure and temperature decreased continuously. With the throttling process increase, the time for the refrigerant to receive the friction resistance of the pipe wall was expanded, so the outlet refrigerant mass flow and jet velocity at the nozzle, the COP of the refrigerant cycle were reduced. All of the average increase rates were -32.529 kPa/m, -2.011°C/m, -0.0467 kg/(s·m), -14.305 s^{-1} and -30.846 m^{-1}, respectively. In the second stage refrigeration cycle, the relationships between instantaneous COP, capillary outlet temperature and corresponding injection speed and pressure were shown in Figure 9.

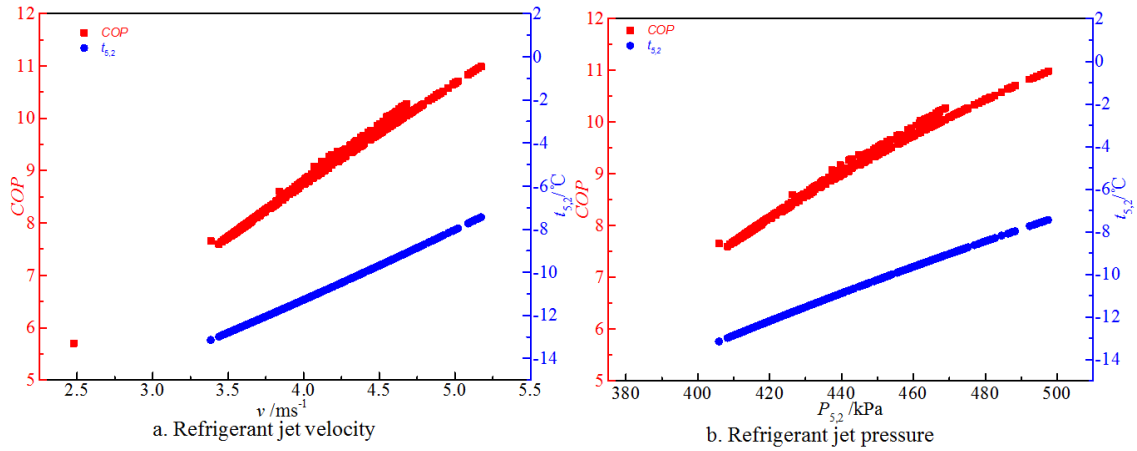

a. Refrigerant jet velocity b. Refrigerant jet pressure

Figure 9. *Variation of refrigeration characteristics parameters with injection temperature and pressure in direction refrigeration process.*

The research results in Figure 9 revealed that both refrigeration COP and capillary outlet temperature had linear increasing trend with the increase of jet velocity and pressure. An important conclusion was drawn that the influence of injection characteristics parameters on COP was greater than the throttling outlet temperature. Moreover, during the refrigeration process, the injection speed and pressure of COP were relatively concentrated in the range of 4.0-4.5 m/s, 440-470 kPa, respectively. The effects of refrigerant injection speed on refrigeration efficiency and outlet temperature caused by the change of capillary parameters were also analyzed in detail. According to the above analysis, the jet velocity increased with the increase of capillary inner diameter and shortening of capillary length. But the injection pressure decreased with the increase of inner diameter. Therefore, the effects of injection speed and pressure on COP and outlet temperature were just the opposite. The research results were shown in Figure 10a and Figure 11a.

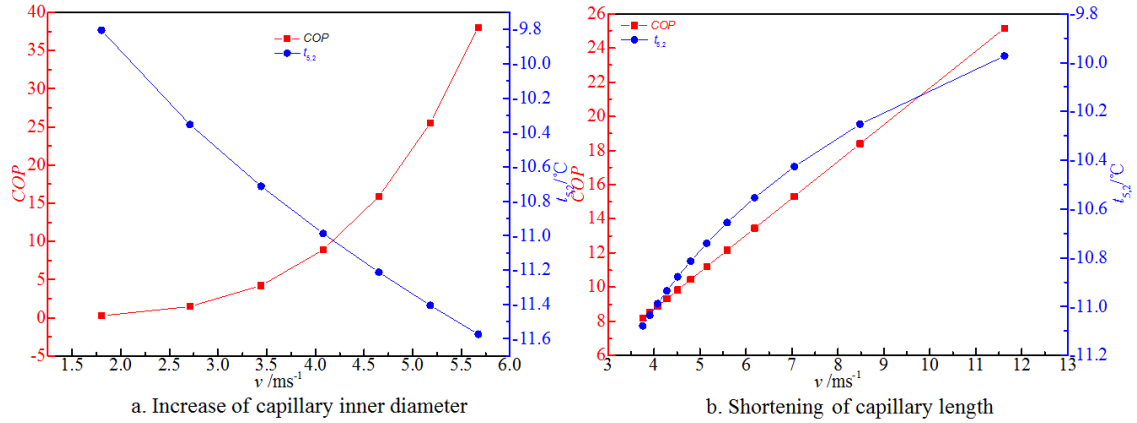

a. Increase of capillary inner diameter b. Shortening of capillary length

Figure 10. *Effect of refrigerant jet velocity on refrigeration characteristics.*

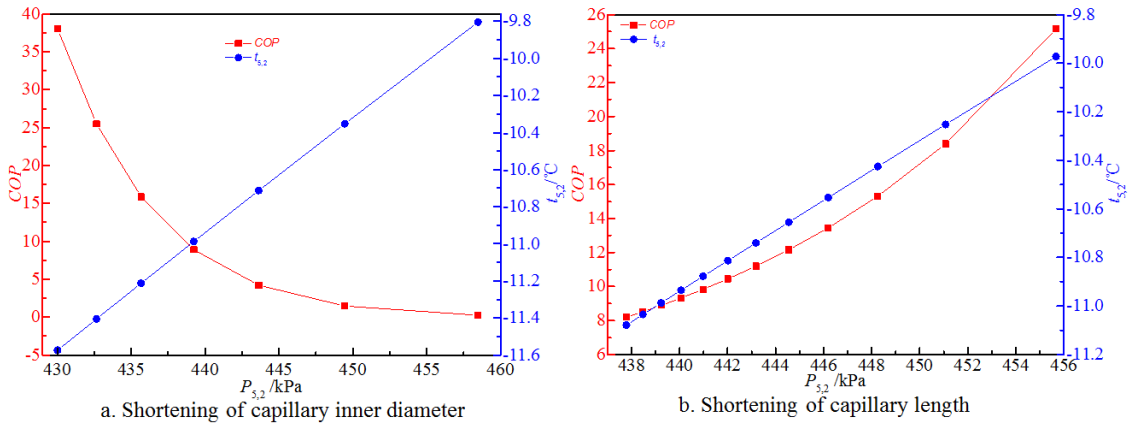

Figure 11. *Effect of refrigerant injection pressure on refrigeration characteristics.*

It was obvious that the capillary inner diameter has the opposite effect on COP and injection temperature. In Figure 10a, by increasing the capillary inner diameter, the refrigerant jet velocity increased and the COP was improved. Moreover, the outlet temperature was reduced, which were beneficial to the refrigeration performance. The average influence rates of jet velocity on COP and outlet temperature were 9.76 $(m \cdot s)^{-1}$ and -0.46°C/$(m \cdot s^{-1})$, respectively. The jet pressure increased along with the decrease of capillary inner diameter. So the COP decreased and the outlet temperature increased in Figure 11a. The average influence rates of jet pressure on COP and outlet temperature were -1.33 $(kPa)^{-1}$ and -0.06°C/kPa, respectively. As shown in Figure 8b, the length of capillary also had a certain influence on the jet velocity and pressure, which increased along with the increase of capillary length. So the research results about the influences of the change of jet velocity and pressure, caused by the change of capillary length, on the COP and outlet temperature of the refrigeration system were shown in Figure 10b and Figure 11b.

Refrigerant jet velocity and pressure were inversely proportional to the capillary length. So shortening the length of the capillary can increase the velocity and pressure Figure 10 and Figure 11 showed that the COP and outlet temperature increased along the increase of jet velocity and pressure. In Figure 10b, the COP increased nearly linearly with the jet velocity and the increase rate of outlet temperature increased first and then decreased. The average increase rates of them were 2.16 $(m \cdot s^{-1})^{-1}$ and 0.14°C/$(m \cdot s^{-1})$, respectively. On the contrary, the outlet temperature increased nearly linearly with the jet pressure and the increase rate of COP decreased first and then increased. The average increase rates of them were 0.06°C/kPa and 0.95 $(kPa)^{-1}$, respectively.

In conclusion, appropriately increasing capillary inner diameter was conducive to improve COP and low temperature liquid refrigerant was obtained. The results also showed that the system had better comprehensive performance when the inner diameter was between 1.5 mm and 2.5 mm. Moreover, the COP was improved but the outlet fluid temperature decreased by shortening capillary length. So the capillary length should be adjusted according to the performance of refrigerator and demand of cooling load. In refrigerant direct injection refrigeration cycle, 40-50 cm capillary length was a better choice.

Refrigerant is not only the core component of refrigeration cycle, but also the main energy transfer medium. The refrigerants had different thermophysical properties due to its different composition. There are many kinds of refrigerants, but R22 (CHClF2) and R134a (CH2FCF3) account for a large market share at present. R22 is a kind of Freona. Because a Chlorine atom is contained in its molecular formula, R22 has destructive effect on the ozone in the earth`s atmosphere. It will be completely eliminated by 2030 according to the Montreal protocol. Because the ozone destruction potential (ODP) of R134a, R407C and R410A were zero. So they do not destroy the ozone layer, which are an environmentally friendly refrigerant recognized and recommended by most countries in the world. But their global warming potential (GWP) are high, which are the causes of global warming. More and more environmentally friendly and zero GWP refrigerants will be researched and developed in the future. In the reported references about refrigerant direct injection refrigeration system, non-environmental friendly refrigerants such R12 and R22 were employed. The research on environmentally friendly refrigerants has not been seen. So in the second stage refrigerant direct injection refrigeration cycle, the refrigeration characteristics of different refrigerants were investigated in this paper. Four common refrigerants R22, R134a, R407 and R410a were selected as the direct injection refrigerants. The results were shown in Figure 12.

It was obvious that the COPs of four refrigerants direct injection in the second stage refrigeration increased sharply to the maximum value and then slowly decreased to the stable value. The period of COP rapid increase was the stage of producing cold water while the period of COP slow decrease was the stage of producing dynamic foam ice. The COP of R410a was the highest with the 8.52 average value and the COP of R134a was the minimum value with the 4.52 average value. The COP of R407C was higher than that of R22, and their average values were 6.13 and 5.56, respectively. R410a was a kind of refrigerant suitable for direct heat exchanger refrigeration cycle.

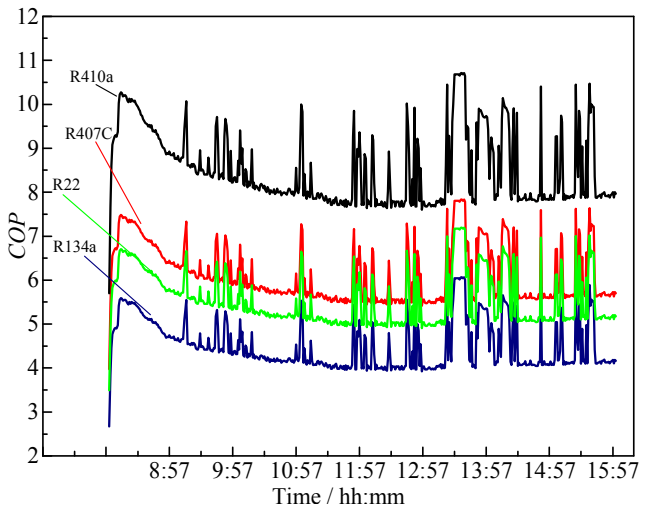

Figure 12. *COPs of fourth refrigerants in the second stage refrigerant injection refrigeration cycle.*

5. Conclusion

A 2kW dynamic two-stage refrigerant direct injection refrigeration system directly driven by DPES was investigated by combining experiment and simulation. Some main results were shown as follows.

(1) Under the typical sunny conditions, the instantaneous generation power and COP tested by experiment, were 15.222 kW·h and 2.479 and the calculated values were 15.066 kW·h and 2.607, respectively. the relative errors of them were -1.03% and 5.16%, respectively. So the model constructed in this paper can be used to analyze dynamic two-stage refrigerant direct injection refrigeration system.

(2) Driven by power grid, the experimental results revealed that the average COPs of injection refrigeration system with R22, R134a and R318 refrigerant were 6.16, 5.80 and 8.70, respectively. And the nozzle outlet temperatures of R22, R134a and R318 were -17.29°C, -10.02°C and -5.09°C, respectively. When directly driven by DPES, the average COPs of R22, R134a, R407C and R410a in the second refrigerant direct injection refrigeration cycle were 5.56, 4.52, 6.13 and 8.52, respectively.

(3) The wall thickness of the plate heat exchanger had a negative effect on the heat transfer coefficient of the exchanger and the COP the second refrigeration system and the average increase rates were - 0.234 kW/(m^2°C) and -0.017, respectively. The higher thermal conductivity of the plate heat exchanger, the better heat transfer performance. But the exchanger price is also expensive. Lead zinc plate heat exchanger with medium thermal conductivity was usually employed in engineering. The exchange area of exchanger had a positive effect on the COP and refrigerant mass flow of the second refrigeration system and average increase rates were 12.92 m^{-2} and 0.0209 kg/(s·m^2), respectively.

(4) The average influence rates of jet velocity caused by changing the inner diameter on COP and outlet temperature were 9.76 $(m·s)^{-1}$ and -0.46°C/$(m·s^{-1})$, respectively. The average influence rates of jet pressure caused by changing the inner diameter on COP and outlet temperature were -1.33 $(kPa)^{-1}$ and -0.06°C/kPa, respectively. Refrigerant jet velocity and pressure were inversely proportional to the capillary length. the COP increased nearly linearly with the jet velocity and the increase rate of outlet temperature increased first and then decreased. The average increase rates of them were 2.16 $(m·s^{-1})^{-1}$ and 0.14°C/$(m·s^{-1})$, respectively. On the contrary, the outlet temperature increased nearly linearly with the jet pressure and the increase rate of COP decreased first and then increased. The average increase rates of them were 0.06°C/kPa and 0.95 $(kPa)^{-1}$, respectively.

Acknowledgements

The authors gratefully acknowledge the financial support provided by National Natural Science Foundation of China (51966019) and Major Science and Technology Special Project of Yunnan (Grant No. 202002AF080002). The research work was also supported by Jiaxing public welfare project (2020AY10019).

References

[1] A. Allouhi, T. Kousksou, A. Jamil, P. Bruel, Y. Mourad, Y. Zeraouli. Solar driven cooling systems: An updated review [J]. Renewable Sustainable Energy Reviews, 2015, 44: 159-181.

[2] M. I. H. Khan, H. M. M. Afroz, M. A. Karim. Effect of PCM on temperature fluctuation during the door opening of a household refrigerator [J]. International Journal of Green Energy, 2017, 14 (4): 379-384.

[3] J. Karwacki. Cooling system with PCM storage for an office building: experimental investigation aided by a model of the office thermal dynamics [J]. Materials, 2021, 14 (6): 1356.

[4] F. Souayfane, F. Fardoun, P. H. Biwole. Phase change materials (PCM) for cooling applications in buildings: A review [J]. Energy and Buildings. 2016, 129: 396-431.

[5] S. F. Li, Z. H. Liu, X. J. Wang. A comprehensive review on positive cold energy storage technologies and applications in air conditioning with phase change materials [J]. Applied Energy, 2019, 255, 113667.

[6] Y. Sun, S. Wang, F. Xiao, D. Gao. Peak load shifting control using different cold thermal energy storage facilities in commercial buildings: A review [J]. Energy Conversion and Management, 2013, 71, 110-114.

[7] G. Yan, Y. Liu, S. X. Qian, J. L. Yu. Theoretical study on a vapor compression refrigeration system with storage for freezer applications [J]. Applied Thermal Engineering, 2019, 160, 114091.

[8] S. Ozgun, K. Husnu, K. Lutfullah. A study on optimizing the energy consumption of a cold storage cabinet [J]. Applied Thermal Engineering, 2017, 112, 424-430.

[9] J. Riffat, C. Kutlu, E. T. Brito, S. Tekpetey, F. B. Agyenim, Y. H. Su, S. Riffat. Development and testing of a PCM enhanced domestic refrigerator with use of miniature DC compressor for weak/off grid locations [J]. International Journal of Green Energy, 2021, 5: 1-14.

[10] G. Y. Fang, F. Tang, L. Cao. Dynamic characteristics of cool thermal energy storage systems—a review [J]. International Journal of Green Energy, 2016, 13 (1): 1-13.

[11] A. S. Baqir, H. B. Mahood, A. N. Campbell, A. J. Griffiths. Measuring the average volumetric heat transfer coefficient of a liquid-liquid-vapour direct contact heat exchanger [J]. Applied Thermal Engineering, 2016, 103: 47-55.

[12] Y. F. Xu, X. Ma, R. H. E. Hassanien, X. Luo, G. L. Li, M. Li. Performance analysis of static ice refrigeration air conditioning system driven by household distributed photovoltaic energy system [J]. Solar Energy, 2017, 158: 147-160.

[13] Y. F. Xu, M. Li, X. Luo, X Ma, Y. F. Wang, G. L. Li, R. H. E. Hassanien. Experimental Investigation of Solar Photovoltaic Operated Ice Thermal Storage Air-conditioning System [J]. International Journal of Refrigeration, 2018, 86: 258-272.

[14] H. B. Mahood, A. N. Campbell, R. B. Thorpe, A. O. Sharif, Heat transfer efficiency and capital cost evaluation of a three-phase direct contact heat exchanger for the utilization of low-grade energy sources [J]. Energy Conversion and management, 2015, 106, 101–109.

[15] H. B. Mahood, R. B. Thorpe, A. N. Campbell, A. O. Sharif, Experimental measurements and theoretical prediction for the transient characteristic of a three-phase direct contact condenser [J]. Applied Thermal Engineering, 2015, 87, 161–174.

[16] Z. Peng, W. Yiping, G. Cuili, W. Kun. Heat transfer in gas–liquid–liquid three phase direct-contact exchanger [J]. Chemical Engineering Journal, 2001, 84 (3): 381–388.

[17] S. Kunkel, T. Teumer, P. Dornhofer, K. Schlachter, Y. Weldeslasie, M. Kuhr, M. Radle, J. U. Repke. Determination of heat transfer coefficients in direct contact latent heat storage systems [J]. Applied Thermal Engineering, 2018, 145, 71–79.

[18] A. Nuntaphan. Performance analysis of a refrigeration cycle using a direct contact evaporator [D], Chiang Mai University, Thailand, 1998.

[19] T. Kiatsiriroat, P. Siriplubpla, A. Nuntaphan, Performance analysis of a refrigeration cycle using a direct contact evaporator [J]. International Journal of Energy Research, 1998, 22, 1179–1190.

[20] A. N. Leiper, D. D. ASH, D. J. Mcbryde, Improving the thermal efficiency of ice slurry production through comminution [J]. International Journal of Refrigeration, 2012, 35 (5): 1931-1939.

[21] S. C. Liu, L. Hao, Z. M. Rao, X. X. Zhang. Experimental study on crystallization process and prediction for the latent heat of ice slurry generation based sodium chloride solution [J]. Applied Energy, 2017, 185, 1948-1953.

[22] K. Hayashi, K. E. Kasza. Ice slurry cooling research: effects of microscale ice particle characteristics and freezing-point depressant additives on ice slurry fluidity [M]. ASHRAE Trans, Part 1 2001, 107: 346–3451.

[23] G. L. Bauerle, R. C. Ahlert. Heat transfer and holdup phenomena in spray column [J]. Ind. Eng. Chem. Process Des. Dev. 4 (2) (1965) 225–230.

[24] H. B. Mahood, A. N. Campell, A. O. Sharif, R. B. Thorpe. Heat transfer measurement in a three-phase direct contact condenser under flooding conditions [J]. Applied Thermal Engineering, 2016, 95, 106–114.

[25] H. B. Mahood, A. O. Sharif, S. Al-aibi, D. Hwakis, R. B. Thorpe. Analytical solution and experimental measurements for temperatures distribution prediction of three-phase direct contact condenser [J]. Energy, 2014, 67, 538–547.

[26] H. B. Mahood, A. O. Sharif, R. B. Thorpe. Transient volumetric heat transfer coefficient prediction of a three-phase direct contact condenser [J]. International Journal of Heat and Mass Transfer, 2015, 51 (2): 165–170.

[27] Rajapakse A, Chungpaibulpatana S. Dynamic simulation of a photovoltaic refrigeration system [J]. RERIC, 1994, 16 (3): 67-101.

[28] Rabl A. Active solar collectors and their applications [M]. USA: Oxford University Press, 1985.

[29] J. P. Laboratory. Theremal performance testing and analysis of photovoltaic modules in natural sunlight [C]. California Institute of Technology, Pasadena, CA, 1976.

[30] T Kiatsirirot, K Thalang, S Dabbhasuta. Ice formation around a jet stream of refrigerant [J]. Energy Conversion and Management, 2000, 41: 213-221.

[31] S. Sideman, Y. Gat, Direct contact heat transfer with change of phase: spray column study of three phase heat exchanger, AICHE Journal, 199612 (2): 1206-1213.

[32] C. K. Blair. Heat transfer characteristics of a three-phase volume boiler direct contact heat exchanger, M. S. Thesis, University of Utha, Salt Lake City, (1976).